ISSN 1063-7826, Semiconductors, 2020, Vol. 54, No. 7, pp. 796–802. © Pleiades Publishing, Ltd., 2020.
Russian Text © The Author(s), 2020, published in Fizika i Tekhnika Poluprovodnikov, 2020, Vol. 54, No. 7, pp. 677–683.

PHYSICS OF SEMICONDUCTOR DEVICES

Photodiodes for Detecting the Emission of Quantum-Sized Disc Lasers Operating in the Whispering Gallery Modes (2.2–2.3 μm)

E. V. Kunitsyna[a],*, M. A. Royz[b], I. A. Andreev[a], E. A. Grebenshchikova[a], A. A. Pivovarova[a], M. Ahmetoglu (Afrailov)[c], Ya. V. Lebiadok[d], R. Yu. Mikulich[d], N. D. Iliinskaya[a], and Yu. P. Yakovlev[a]

[a] *Ioffe Institute, St. Petersburg, 194021 Russia*
[b] *University of Helsinki, Helsinki, 00014 Finland*
[c] *Department of Physics, Uludag University, Gorukle, Bursa, 16059 Turkey*
[d] *GNPO "Optics, Optoelectronics and Laser Technology", National Academy of Sciences of Belarus, Minsk, 220072 Belarus*
**e-mail: kunits@iropt9.ioffe.ru*

Received February 25, 2020; revised February 28, 2020; accepted February 28, 2020

Abstract—Photodiodes based on solid solutions in the GaSb–InAs system are for the first time applied to study the spectral characteristics of single and coupled whispering-gallery-mode (WGM) lasers emitting in a range of 2.2–2.3 μm. The capacity of photodiodes with a photosensitive area 2.0 mm in diameter is C = 520 pF at $U = -2$ V, which corresponds to a time constant of $\tau = 53$ ns. It is shown that the parameters of the fabricated photodiodes make it possible to detect the emission of quantum-sized disc lasers at room temperature not using cryogenic cooling.

Keywords: photodiodes, GaSb/GaInAsSb/GaAlAsSb heterostructures, quantum-sized disc lasers, WGM modes

DOI: 10.1134/S1063782620070052

1. INTRODUCTION

New designs of semiconductor lasers operating in whispering gallery modes (WGM) in the mid IR-range at room temperature and near-room temperatures have been developed over the last decade [1, 2]. A distinctive feature of such lasers is the use of a disc cavity with a high figure of merit, which makes it possible to apply materials with low optical amplification. In addition to a high figure of merit, disc WGM lasers show lower threshold currents and an extended frequency tuning range when compared with stripe lasers [2], which make them promising for the development of optical frequency standards.

It is known that the detection of laser radiation in the spectral range of 2–3 μm is not a simple scientific and practical problem. Semiconductor photodetectors based on lead chalcogenides are used in this wavelength range. Their detectability under light cooling is currently approaching the theoretical limit [3]. However, the time constant of most photodetectors based on these materials is 100–400 μs. The authors of [4] reported the fabrication of fast-response photodetectors based on CdPbS solid solutions for wavelengths of 2.1–2.4 μm with the time constant τ = 20–50 μs as well as photodetectors based on an especially pure PbS film with τ = 5–70 μs at T = 295 K. The authors of [5] developed a PbS-based photoresistor that has spectral sensitivity in the range 0.4–3.0 μm and τ = 3–5 μs. Such devices with record parameters are in demand in various fields of science and technology; however, a substantially more rapid response speed is required for operation with lasers. It should be noted that promising materials for the next generation of photodetectors are PbS and PbSe quantum dots including colloidal quantum dots, and intensive investigations are being performed in this direction [6–8].

Other widely applied photodetectors, including those operating in the range near 3 μm, are InSb-based photodiodes [9]. A detailed review of the manufacturing aspects of growing materials for InSb-based photodiodes by the MBE and MOCVD methods on Si and GaAs substrates is given by Razeghi [10]. One new direction in the field of designing highly sensitive nanoscale devices is investigation into the photoelectric properties of "metal–semiconductor–metal" InSb nanowire-based structures [11]. Investigations with the purpose of fabricating HOT-InSb photodetectors for detecting room temperature IR radiation have been developed in recent years [12]. New possibilities in this field, as it was shown theoretically, have been opened up by the design of nonequilibrium p–i–n InSb photodiodes with a detectability reaching 3×10^9 cm $Hz^{1/2}$ W^{-1} (T = 300 K) in the spectral region up to 8 μm [13]. The application of uncooled InSb-based photodiodes with a sensitivity in

Table 1. Parameters of epitaxial layers for GaSb/GaInAsSb/GaAlAsSb photodiode structures

Composition	Conductivity type	Doping impurity	Growth temperature, °C	Thickness, μm
$Ga_{0.78}In_{0.22}As_{0.18}Sb_{0.82}$	*n*	Te	600	2.0–2.5
$Ga_{0.66}Al_{0.34}As_{0.025}Sb_{0.975}$	*p*	Ge	599	1.5–2.0

the range of 2–7 μm combined in a series was reported for the development of a sensor of such gases as CO_2, CO, and NO_x [14]. However, cooling to 80–200 K is required for the effective operation of most InSb-based photodiodes.

In this work, we consider the possibility of the application of photodiodes designed on the basis of solid solutions in the GaSb–InAs system for detection of the emission of quantum-sized disc WGM lasers with a wavelength of 2.2–2.3 μm at room temperature.

2. DESIGN OF THE EXPERIMENTAL SAMPLES AND INVESTIGATION PROCEDURES

Single- and coupled-disc WGM lasers were fabricated on the basis of a quantum-sized GaInAsSb/GaAlAsSb heterostructure, the growth of which is described in [15], by photolithography and liquid chemical etching. The cavity diameter was 400 μm and its height was about 3 μm, while the mesa height was 7 μm. A face ohmic contact in the shape of a ring was formed using explosive photolithography and high-vacuum thermal deposition of the Cr/Au/Ni/Au system. Then the face contact was thickened by the selective electrochemical deposition of Au. To form a continuous ohmic contact on the side of the GaSb substrate, we sequentially deposited Cr/Au/Ni/Au and Cr/Au systems. The contacts were burnt-in in a hydrogen atmosphere at 300°C. The laser chips were mounted in a standard TO-18 case.

Photodiodes were fabricated based on *n*-GaSb/*n*-GaInAsSb/*p*-GaAlAsSb heterostructures. These heterostructures were LPE grown on *n*-GaSb(100) substrates doped with tellurium to a carrier concentration of $(1–5) \times 10^{17}$ cm^{-3}. The absorption region was the epitaxial layer of the narrow-gap $GaIn_{0.22}AsSb$ solid solution (E_g = 0.53 eV) 2.0–2.5 μm in thickness (see Table 1). The $GaAl_{0.34}AsSb$ epitaxial layers (E_g = 1.1 eV) 1.5–2.0 μm in thickness were used as a "wide-gap window". When growing Al-containing layers, the saturating single-crystal GaAs substrate contacting with the melt was used for the introduction of As into the melt during homogenization. The As concentration in the melt in the case of applying this two-phase method is determined by temperature and is almost independent of the content of the other components.

The effective separation of carriers is provided when forming a rather broad space-charge region in GaSb/GaInAsSb/GaAlAsSb photodiode heterostructures. The classical *p–i–n* photodiode includes an *i*-type region with a carrier concentration close to intrinsic in the selected material. A space-charge region with the width W and built-in field with the strength $E(x)$ is formed in the epitaxial *i*-type layer with the thickness d under reverse bias U_{rev}. Applied U_{rev} should be sufficient to deplete th *i*-type layer and provide the conditions $W \le d$. On the other hand, the condition $\alpha W \gg 1$, where α is the material absorption coefficient, should be fulfilled for complete emission absorption in the active layer. The absorption coefficient α in direct-gap semiconductors, in particular, in the GaInAsSb solid solution, exceeds 10^4 cm^{-1} for emission with a quantum energy larger than E_g of the material. In this case, W should be several μm; therefore, selection of the thickness of the active GaInAsSb region of 2–3 μm provides almost complete absorption of the incident radiation.

The GaInAsSb active region was doped with tellurium to the concentration $n = (2–5) \times 10^{16}$ cm^{-3}, and the GaAlAsSb "wide-gap window" was doped with germanium to the concentration $p = (6–8) \times 10^{18}$ cm^{-3}. When doping $Ga_{0.78}In_{0.22}As_{0.18}Sb_{0.82}$ solid solutions with tellurium, it is possible to fabricate a material of *n*-type conductivity. Herewith, the degree of compensation of the semiconductor is determined as

$$\frac{N_D + N_A}{N_D - N_A},$$

where N_A is the native acceptor concentration and N_D is the uncompensated donor concentration [16]. In the material of the active region of the studied photodiodes, $N_A \sim 2 \times 10^{17}$ cm^{-3} and $N_D - N_A = (2–5) \times 10^{16}$ cm^{-3}, then $K \sim 10$.

When fabricating photodiodes, it should be taken into account that the high degree of compensation of the active-region material leads to growth of the generation–recombination component of the dark current. This effect in compensated semiconductors is due to lowering of the effective carrier lifetime in the bulk charge layer τ_{eff} when compared with pure materials. The high degree of compensation at large reverse biases U_{rev} corresponding to electric fields with a strength on the order of $E \sim 10^4–10^5$ V/cm leads to an increase in the tunneling component of the dark current, which is due to tunneling through the energy states in the band gap. It is known that the electric-field fluctuations caused by doping nonuniformities are directly proportional to the degree of compensation K of the material. In this case, when doping

GaInAsSb solid solutions by tellurium even to the concentration $n = 2 \times 10^{16}$ cm^{-3} ($K = 10$), the electric-field fluctuations are an order of magnitude higher than in heterostructures based on pure material. Thus, a further decrease in the concentration in the active GaInAsSb region due to the doping impurity leads to an increase in the dark current and strong electric-field fluctuations. To solve this problem, it is necessary to use such methods as growth using rare-earth elements or neutral solvent [16].

Chips with diameters of the photosensitive area of 0.5, 2, and 2.8 μm were fabricated from the grown photodiode GaSb/GaInAsSb/GaAlAsSb heterostructures by contact photolithography and liquid chemical etching. To protect the lateral surface of the mesa and *p–n* junction, anodic oxide which formed in the electrolyte solution (0.3% tartaric acid/ethylene glycol in the ratio 1:2) was used. The thickness of the oxide formed at $U = 60$ V and $j = 5$ mA/cm^2 was ~0.3 μm.

The Cr/Au/Ni/Au system and a galvanic Au layer formed by selective electrochemical deposition were used as a contact system to the Al-containing epitaxial layer of *p*-type conductivity. Such contact enhancement makes it possible to assemble photodiodes by soldering at elevated solder temperatures of 200–230°C. A continuous contact to the *n*-GaSb substrate was formed by sputtering the Cr/Au/Ni/Au system with subsequent sputtering of an additional Cr/Au layer to implement the assembly. The face contact for photodiodes with photosensitive areas 0.5 and 2.0 mm in diameter was created in the form of a ring (Fig. 1a). However, a cross-shaped contact, which made it possible to collect the photocurrent more rapidly, was used with a larger diameter of the photosensitive area of 2.8 mm (Fig. 1b). The selected contact corresponded to the optimal ratio of the formed photocurrent and degree of shadowing. Photodiode chips were mounted into TO-5 cases with a frigistor to establish and maintain the temperature from –70°C to +100°C.

The current–voltage (I–V) characteristics of the photodiodes were investigated using an automated meter of the I–V characteristics. The plots were displayed on a computer monitor in real time. The photosensitivity spectra of the photodiode samples under study were measured according to a synchronous-detection circuit using an SPM prism monochromator (Carl Zeiss), mechanical modulator, and Stanford Research SR830 synchronous detector. To determine the current monochromatic sensitivity $S_I(\lambda_{max})$, a method of comparison with a calibrated radiation detector was used.

The spectral characteristics of WGM lasers were investigated using an installation including a DK-480 monochromator (CVI Laser Corp.) at room temperature in the pulsed-supply mode. A PA-9 device produced by Judson Technologies was used as a preliminary amplifier. A synchronous detection circuit using a Stanford Research SR810 device was applied. The spectra of the WGM lasers were investigated at various pump currents. The fabricated GaSb/GaInAsSb/GaAlAsSb photodiodes were used as detectors of laser emission.

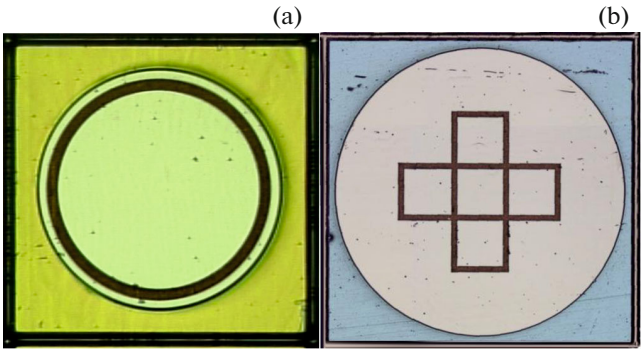


Fig. 1. Microphotograph of photodiode chips with a photosensitive area (a) 2.0 mm in diameter and (b) 2.8 mm in diameter formed on the basis of GaSb/GaInAsSb/GaAlAsSb heterostructures.

3. EXPERIMENTAL RESULTS AND DISCUSSION

The distribution of the spectral sensitivity of GaSb/GaInAsSb/GaAlAsSb photodiodes is presented in Fig. 2. The long-wavelength boundary of the spectral sensitivity $\lambda = 2.4$ μm at room temperature is determined by the band-gap width of the active region. It is seen from Fig. 2a that the half-decay wavelength of the spectral characteristic $\lambda_{50\%} = 2.32$ μm. Then the band-gap width of the direct-gap $GaIn_{0.22}AsSb$ solid solution in the active photodiode region calculated from $\lambda_{50\%}$ is $E_g = 0.53$ eV, which agrees completely with the photoluminescence data. When determining E_g from the results of measurement of the current–voltage characteristics of the photodiodes at two temperatures according to the method proposed in [17] initially for the semiconductor *p–n* homostructures, we found a close value of $E_g = 0.535$ eV. Thus, we assume that this method can be applied to evaluate E_g of the active region of narrow-gap GaSb-based heterostructures with an error of ~1%.

The sensitivity gradually decreases in the shorter-wavelength part of the spectrum towards short wavelengths, which is associated with absorption at indirect-gap transitions in the layer of the Al-containing solid solution. The short-wavelength spectral sensitivity boundary, which is determined by the band-gap width of the "wide-gap window" is $\lambda = 1.12$ μm at $T = 300$ K.

The current monochromatic photosensitivity of GaInAsSb/GaAlAsSb photodiodes at the spectral characteristic maximum ($\lambda = 2.0$–2.3 μm) is $S_I = 0.7$–

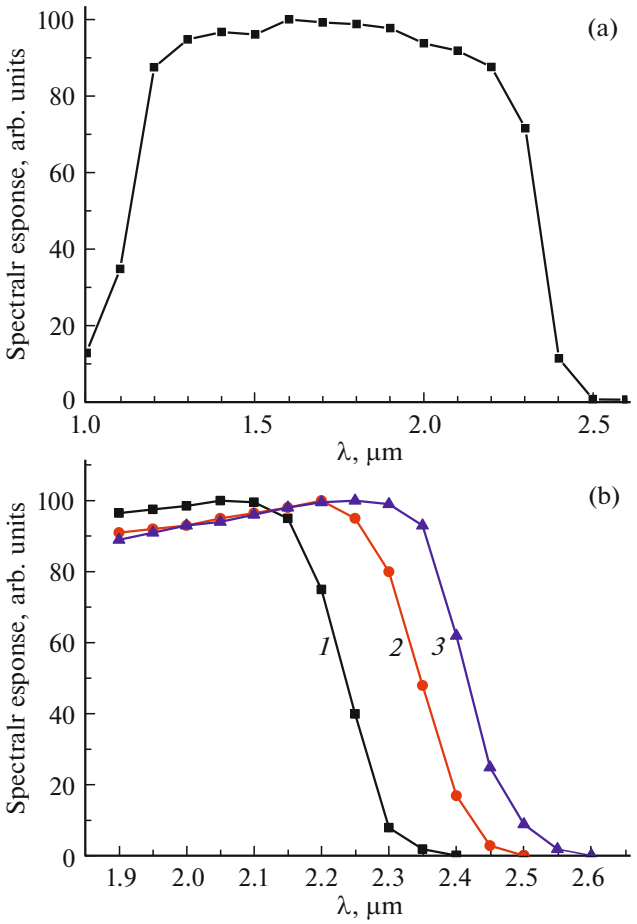


Fig. 2. Distribution of the spectral sensitivity of GaInAsSb/GaAlAsSb photodiodes: (a) at room temperature and (b) at various temperatures, T: (*1*) 253, (*2*) 296, and (*3*) 313 K.

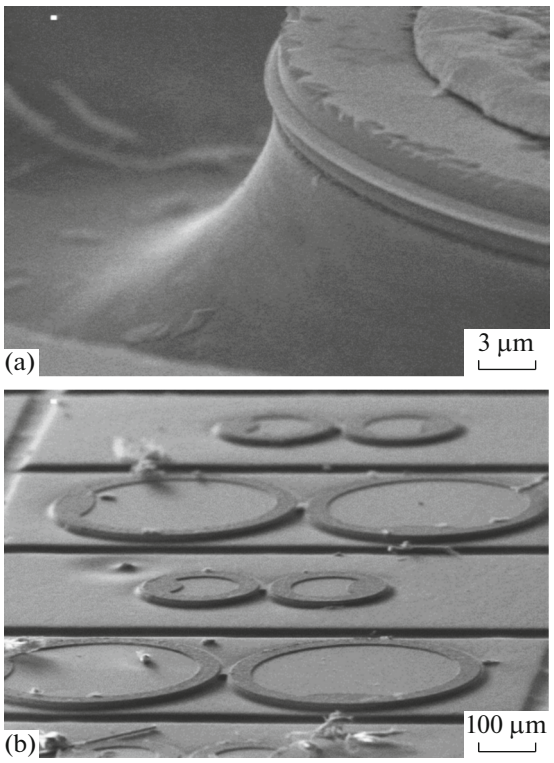


Fig. 3. SEM images of the semiconductor WGM lasers: (a) cavity side surface and (b) coupled lasers with cavities 400 and 200 μm in diameter.

1.0 A/W, which corresponds to the quantum efficiency $\eta = 0.5–0.7$.

It is seen from Fig. 2b that the long-wavelength spectral sensitivity boundary shifts towards shorter wavelengths with a decrease in temperature. The coefficient of temperature variation in the wavelength is $\Delta\lambda/\Delta T = 3.3 \times 10^{-3}$ μm/K, which corresponds to the coefficient of the band-gap temperature variation of the active region $\Delta E_g/\Delta T = -7.7 \times 10^{-4}$ eV/K in the temperature range $\Delta T = 60$ K.

Investigation into the capacitance–voltage characteristics shows that the capacity of photodiodes with zero reverse bias ($U_{rev} = 0$ V) is $C = 150$ pF at a photosensitive area of 0.5 mm in diameter, $C = 685$ pF at a diameter of 2.0 mm, and $C = 1380$ pF at a diameter of 2.8 mm, respectively.

We used our GaSb/GaInAsSb/GaAlAsSb photodiodes to investigate the spectral characteristics of single- and coupled-disc WGM lasers based on a quantum-sized GaInAsSb/GaAlAsSb heterostructure. Figure 3a shows an image of the side surface of the cavity recorded using a scanning electron microscope (SEM). The chemical etching of strained and unstrained layers of various compositions proceeds at different rates. Aluminum-containing isoperiodic layers in the GaInAsSb/GaAlAsSb isoperiodic heterostructure are etched faster then the strained layer of GaInAsSb quantum wells, which leads to the formation of a convex part of the cavity waveguide, inside which WGM modes propagate along a circular trajectory. Doubled WGM lasers were fabricated with a conjunction between the cavities (Fig. 3b), the conjunction width is 20–35 μm, the conjunction length is 10–15 μm, and the conjunction height is 7 μm (similarly to the cavity mesa). This design makes it possible to form a strong optical connection between two disc laser cavities because the emission can transfer from one cavity into another through the conjunction not leaving the cavities.

The emission wavelength of the WGM lasers under study was in the range 2.2–2.3 μm. After comparing the parameters of the photodiodes with various diameters of the photosensitive area, samples with an area of 2.0 mm in diameter were selected as detectors for the installation. On the one hand, such photodiodes have a lower level of reverse dark currents and, correspondingly, noise, as well as a smaller capacity (the higher speed response) than devices with an area of 2.8 mm in diameter. On the other hand, they have a

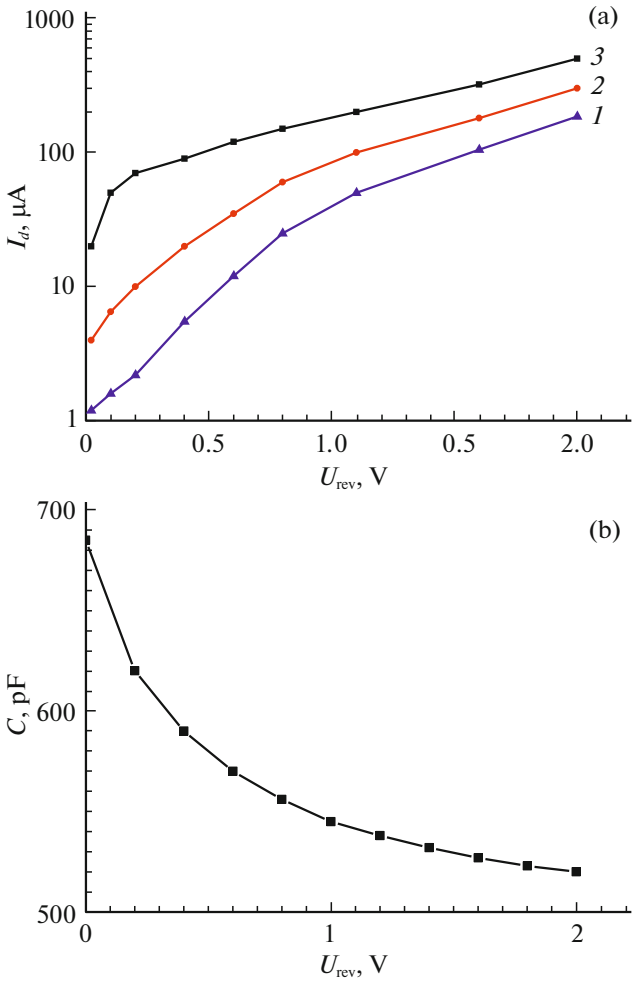


Fig. 4. Electrical characteristics of the GaSb/GaInAsSb/GaAlAsSb photodiode with a sensitive area 2.0 mm in diameter: (a) dependence of the reverse current voltage I_d on the supplied voltage U_{rev} at $T = 173$ (*1*), 263 (*2*), and 296 K (*3*); (b) capacitance–voltage characteristic at $T = 296$ K.

higher spectral sensitivity when compared with photodiodes with an area of 0.5 mm in diameter and are much more convenient for installation tuning when studying lasers.

The dependence of the reverse dark current I_d on the applied voltage U_{rev} at various temperatures for a GaSb/GaInAsSb/GaAlAsSb photodiode with a sensitive area of 2.0 mm in diameter mounted on a thermoelectric module is shown in Fig. 4a. It is seen from Fig. 4a, as U_{rev} increases tenfold at room temperature from 0.2 to 2 V, I_d also increases tenfold, which evidences the increasing influence of the tunneling-current mechanism. The photodiode capacity drops from $C = 685$ pF at $U_{rev} = 0$ V to $C = 520$ pF at $U_{rev} = -2$ V (Fig. 4b), which makes it possible to increase the response speed, or time constant, from $\tau = 75$ to $\tau = 53$ ns.

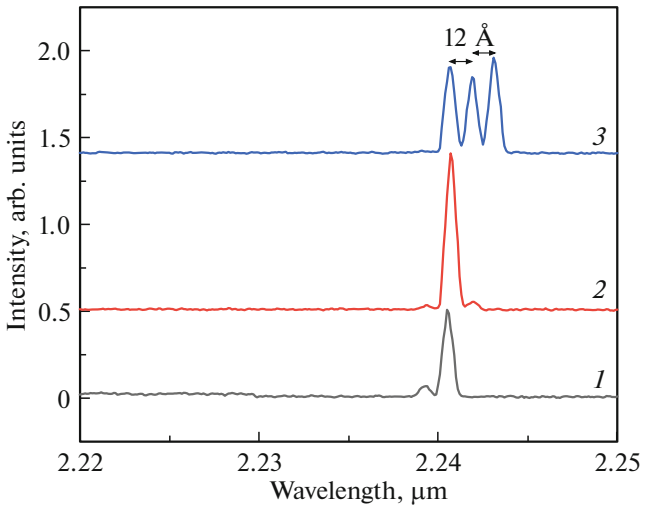


Fig. 5. Emission spectra of a single WGM laser with a disc cavity 400 μm in diameter at room temperature and pump-current densities $I = 175$ (*1*), 180 (*2*), and 200 A/cm^2 (*3*).

The generation of the laser emission of single WGM lasers was excited when supplying rectangular electrical pulses with different frequency and duration. The working frequency range Δf was 2–16 kHz; herewith, the duration of the pulse t_i could vary from 2 to 60 μs. However, optimal laser operation is observed at a pulse-repetition frequency of $f = 10$ kHz and duration of $t_i = 2.7$ μs. These values of the parameters allow us to conserve the position of the generated laser modes in the emission spectra over the entire range of working pump currents, i.e., allow us to avoid the "red shift" effect associated with sample heating.

Figure 5 shows the coherent emission spectrum of a single WGM laser with a cavity 400 μm in diameter at various pump currents recorded using a monochromator with two diffraction grids. Clear equidistant laser modes, the distance between which is ~12 Å, are observed in the emission spectra. This quantity agrees with the value found with the help of a formula for calculating the intermode distance of first-order modes in a WGM laser:

$$\Delta\lambda = \frac{\lambda^2}{2\pi Rn}, \quad (1)$$

where λ is the working wavelength, Δλ is the intermodal distance, R is the cavity radius, and n is the medium refractive index ($n = 3.5$ for our case).

The correspondence of the experimental and calculated values of the intermodal distance Δλ confirms that these lasers operate with first-order whispering gallery modes.

The directivity patterns were measured in the supply mode described above ($f = 10$ kHz, $t_i = 2.7$ μs). In contrast with most of other types of lasers, no directed emission is observed for WGM lasers because the radi-

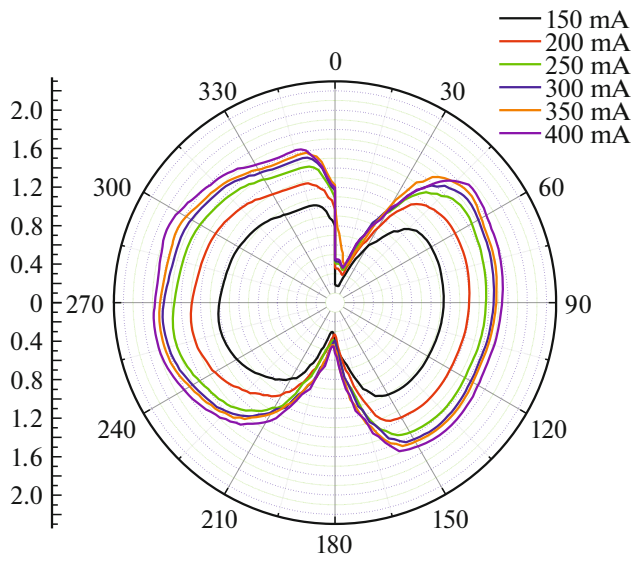


Fig. 6. Emission directivity diagram of a disc WGM laser at pump currents of $I = 150–400$ mA.

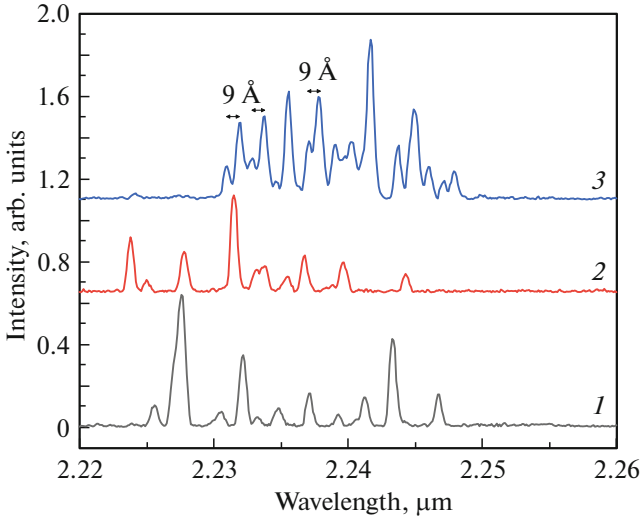


Fig. 7. Emission spectra of doubled WGM lasers with cavities 400 μm in diameter and a conjunction with supply to the first cavity (*1*), to the second cavity (*2*), and to both cavities simultaneously (*3*); the spectra are recorded at room temperature and the pump-current density $I = 250$ A/cm^2.

ation propagates homogeneously in all directions due to scattering at nonuniformities of the waveguide surface. This is clearly observed in the typical directivity diagram of a single disc laser with a cavity of 400 μm in diameter recorded at various pump currents (Fig. 6). It is seen in Fig. 6 that the emission distribution is homogeneous over all directions excluding sectors from 0° to 30° and from 160° to 190°, where the emission-intensity decay is observed. This is associated with the fact that disc WGM lasers were mounted into a standard TO-18 case with two isolated outputs to provide electrical contact. The intensity-decay sectors correspond to the position of these contact outputs.

The emission spectra of coupled WGM lasers with a conjunction between the cavities were also measured using GaSb/GaInAsSb/GaAlAsSb photodiodes. Figure 7 shows the spectra of the laser with coupled cavities 400 μm in diameter. It is seen from Fig. 7 that the spectra of coupled lasers pumped separately (plots *1*, *2*) considerably differ from the case when the lasers operate simultaneously (plot *3*). For example, when supplying the pump current to both lasers, we simultaneously observe numerous new laser modes, which can be attributed to the class of the collective modes of doubled cavities. When compared with the WGM modes of a single laser, the collective modes have a considerably more complex structure and can occur only if their optical path passes through both cavities.

The conjunction of the coupled lasers is relatively wide (35 μm) relative to the cavity diameter, in connection with which, the equidistance of laser lines is violated when lasers operate separately from one another and vanishes in certain cases (Fig. 7, plot *2*). On the other hand, equidistance starts to manifest itself again with the simultaneous operation of lasers, and the number of generated modes increases. The intermodal distance is 9 Å in this case (Fig. 7, plot *3*), which is smaller when compared with the value for a single disc. This fact confirms that the optical path of new "collective modes" in a coupled cavity is longer than the optical path of WGM modes in a single cavity.

4. CONCLUSIONS

The emission spectra of disc WGM lasers based on a quantum-sized GaSb/GaInAsSb/GaAlAsSb heterostructure were for the first time investigated using photodiodes formed also in the system of GaSb–InAs solid solutions. Photodiodes were mounted into cases with a frigistor, which made it possible to establish and maintain the temperature from –20°C to +60°C. A photodiode diameter of 2.0 mm was selected in order to optimally combine the spectral sensitivity, level of reverse dark currents and noise, respectively, the response speed and tuning convenience for devices based on these narrow-gap materials. The capacity of such photodiodes is $C = 520–685$ pF with reverse bias $U_{rev} = -2.0–0$ V, which corresponds to the time constant $\tau = 53–75$ ns. This response speed exceeds that of widely used photodetectors based on lead chalcogenides by 2–3 orders of magnitude. It was shown that GaSb/GaInAsSb/GaAlAsSb photodiodes can be used without cooling to register the emission of single and coupled WGM lasers with the emission wavelength of the fundamental mode in the range of 2.2–2.3 μm.

ACKNOWLEDGMENTS

We thank S.I. Troshkov for the formation of SEM images of semiconductor WGM lasers.

FUNDING

This study was supported by the Russian Foundation for Basic Research, research project no. 18-52-00027 Bel_a. Investigations on the Belarusian side are supported by the Belarusian Foundation for Basic Research, project F18R-121.

CONFLICT OF INTEREST

The authors declare that they have no conflict of interest.

REFERENCES

1. A. N. Imenkov, V. V. Sherstnev, M. A. Sipovskaya, A. P. Astakhova, E. A. Grebenshchikova, A. M. Monakhov, K. V. Kalinina, G. Boissier, R. Teissier, A. N. Baranov, and Yu. P. Yakovlev, Tech. Phys. Lett. **35**, 857 (2009).
2. A. N. Baranov, G. Boissier, R. Teissier, A. M. Monakhov, V. V. Sherstnev, M. I. Larchenkov, and Yu. P. Yakovlev, Appl. Phys. Lett. **100**, 061112 (2012).
3. V. G. Butkevich, V. D. Bochkov, and E. R. Globus, Prikl. Fiz., No. 6, 66 (2001).
4. R. D. Mukhamed'yarov and I. N. Miroshnikova. http://uralsemiconductor.ru/articles/Doklad_Kongress-2017_Ural_fotodetektory_r25.04–21.20%20.pdf.
5. A. V. Shnaider, M. P. Mironov, A. V. Gusel'nikov, V. F. Markov, and L. N. Maskaeva, Pozharovzryvobezopasn., No. 2, 14 (2008).
6. H. Tang, J. Zhong, W. Chen, K. Shi, G. Mei, Y. Zhang, Z. Wen, P. Muller–Buschbaum, D. Wu, K. Wang, and X. Sun, ACS Appl. Nano Mater. **2**, 6135 (2019).
7. M. Thambidurai, Y. Jang, A. Shapiro, G. Yuan, H. Xiaonan, Y. Xuechao, Q. J. Wang, E. Lifshitz, H. V. Demir, and C. Dang, Opt. Mater. Express **7**, 2326 (2017).
8. L. Hu, S. Huang, R. Patterson, and J. Halpert, J. Mater. Chem. C **7**, 4497 (2019).
9. B. W. Jia, K. H. Tan, W. K. Loke, S. Wicaksono, K. H. Lee, and S. F. Yoon, ACS Photon. **5**, 1512 (2018).
10. M. Razeghi, Eur. Phys. J. Appl. Phys. **23**, 149 (2003).
11. C. Kuo, J. Wu, S. Lin, and W. Chang, Nanoscale Res. Lett. **8**, 327 (2013).
12. P. Martyniuk and A. Rogalski, Opto-Electron. Rev. **21**, 239 (2013).
13. C. Shi, Y. Dong, and Q. Li, IEEE Trans. Electron Dev. **66**, 1361 (2019).
14. E. G. Camargo, S. Tokuo, H. Goto, and N. Kuze, Sens. Mater. **26**, 253 (2014).
15. D. A. Yarekha, G. Glastre, A. Perona, Y. Rouillard, F. Genty, E. M. Skouri, G. Boissier, P. Grech, A. Joullie, C. Alibert, and A. N. Baranov, Electron. Lett. **36**, 537 (2000).
16. W. Shockley, Czechosol. J. Phys. B **11**, 81 (1961).
17. T. I. Voronina, T. S. Lagunova, E. V. Kunitsyna, Ya. A. Parkhomenko, D. A. Vasyukov, and Yu. P. Yakovlev, Semiconductors **35**, 904 (2001).
18. I. M. Vikulin, B. V. Korobitsyn, and S. K. Kris'kiv, Semiconductors **50**, 1216 (2016).

Translated by N. Korovin